RESEARCH ARTICLE

PROTEINS WILEY

Interactions of heparin derivatives with recombinant human keratinocyte growth factor: Structural stability and bioactivity effect study

Hourieh Kalhor[1] | Hoda Abolhasani[1,2] | Reyhaneh Kalhor[1,3] |
Tahereh komeili Movahhed[1] | Hamzeh Rahimi[4,5]

[1]Cellular and Molecular Research Center, Qom University of Medical Sciences, Qom, Iran

[2]Department of Pharmacology, School of Medicine, Qom University of Medical Sciences, Qom, Iran

[3]Department of Genetics, Colleague of Sciences, Kazerun Branch, Islamic Azad University, Kazerun, Iran

[4]Molecular Medicine Department, Biotechnology Research Center, Pasteur Institute of Iran, Tehran, Iran

[5]Host-pathogen Interaction Department, Texas Biomedical Research Institute, San Antonio, Texas, USA

Correspondence
Hamzeh Rahimi, Molecular Medicine Department, Biotechnology Research Center, Pasteur Institute of Iran, No. 69, 12th Farwardin St, Tehran, Iran.
Email: rahimi.h1981@gmail.com

Abstract

Heparin and heparan sulfate are important glycosaminoglycans that can regulate the activities of many vital proteins, especially the fibroblast growth factor (FGF) family. Because FGF7 (KGF) has an important role in tissue repair and maintaining the integrity of the mucosal barrier, recombinant human keratinocyte growth factor (rhKGF, palifermin) has been approved for the treatment of wound healing and oral cavity. Due to heparin plays an important role in the KGF signaling pathway, a more detailed study of the drug–drug interactions (DDIs) between rhKGF and heparin at the atomic level and investigating their synergistic effect on each other in terms of biology, especially *in silico*, is necessary for a better understanding of DDIs. In this study, DDIs between rhKGF and low-molecular weight heparin types (LMWH) were investigated. In this regard, scrutiny of the influence of the synergistic heparin types on the structure and biostability of rhKGF is accomplished using computational methods such as molecular docking and molecular dynamic simulations (MDs). Subsequently, the motion behavior of rhKGF in interaction with LMWHs was evaluated based on eigenvectors by using principal component analysis (PCA). Also, the binding free energies of rhKGF-LMWH complexes were calculated by the molecular mechanics/Poisson–Boltzmann surface area (MM-BPSA) method. The result showed that rhKGF-idraparinux (−6.9 kcal/mol) and rhKGF-heparin (−6.0 kcal/mol) complexes had significant binding affinity as well as they had a more stable binding to rhKGF than to other LMWH during 100 ns simulation. However, in order to confirm the curative effect of these drugs, clinical trials must be done.

1 | INTRODUCTION

Heparin and heparan sulfate (HS) are linear polysaccharides belonging to the family of glycosaminiglycans which are composed of α 1-4 linked disaccharide repeating units containing a uronic acid and an amino sugar.[1] Owing to the presence of sulfate groups at specific positions in heparin and HS, they have a high negative charge density, because they can bind to an extensive range of molecules through electrostatic interaction.[2,3] Recently, studies have announced that heparin and HS can regulate biological processes such as cell signaling pathways.[4–6] So far, about 300 HS-binding proteins (HSBPs) have been reported including; growth factors family, cytokines, chemokines, extracellular matrix proteins, enzymes, and cell surface proteins of pathogens.[7] Keratinocyte growth factor (KGF or fibroblast growth factor [FGF]-7) is a unique member of the FGFs family, and is produced by mesenchymal cells. It binds only to an isoform of FGFR2; known as FGFR2IIIb form (KGFR).[8] It is well documented that heparin and HS are obligatory coreceptors that bind KGF to KGFR to regulate the activity and function of KGF through modulating dynamics as well as the kinetics of KGF-KGFR interactions.[9,10] Due to KGF plays a critical role in the development and repair of tissue, a recombinant human KFG (rhKGF or palifermin), is being produced.[11,12] Currently, rhKGF (palifermin) is the only approved pharmacological agent to decrease the incidence and duration of severe oral mucositis (OM) which is administered before and after chemotherapy, radiation, and stem cell therapy.[8] However, the therapeutic applications of rhKGF are limited because of its short half-life and poor stability. Also, this protein unfolds at body temperature (∼37°C), so the unfolded protein aggregates rapidly.[13] It is proven that frequent administration of rhKGF (every day) often results in impaired homeostasis *in vivo* and may cause severe side effects like rash, erythema, edema, and pruritus.[8]

Despite various research efforts, these limiting factors still have been an interesting challenge to cancer researchers and clinicians. So far, different strategies have been employed to improve the stability, activity, and quality of rhKGF including, more effective expression systems, construct engineering, and protein engineering.[14–16] It is reported that solid-phase PEGylating can significantly improve the biostability of KGF without affecting its native structure.[17,18] There is evidence that suggests several type of polyanions including heparin, inositol hexaphosphate (IHP), and sucrose octasulfate (SOS) which cause to more stability of the KGF through increasing the thermal-unfolding temperature.[19] It is well determined that the main reason for the instability and aggregation problem of rhKGF is the positive charge patch. So some of the previous studies have used compounds with negative charge like citrate and sulfated polysaccharides, especially heparin and dextran sulfate, as well as low molecular weight additives such as osmolytes and salts to decrease the rate of rhKGF's aggregation and increase the rhKGF's half-life.[13,20,21] On the other hand, numerous studies have shown that there is a potential pharmacokinetic relationship between different types of heparin and rhKGF. Moreover, it is well-approved that if rhKGF and heparins are administrated simultaneously, it can significantly increase the rhKGF's AUC (actual body exposure, area under the curve) up to fivefold while the rhKGF's CL (total body clearance) and Vss (volume of distribution at steady-state) as well as half-life remarkable decrease.[22] Also, it is hypothesized that coadministration rhKGF and heparin may increase the stability and bioactivity of rhKGF. So far, the drug–drug interactions (DDIs) between rhKGF and heparin have been studied at the clinical level. However, there is no exact details about the interaction of rhKGF with heparin on the atomic level and it has still remained a serious challenge. On the other hand, the studies show that the compounds with negative charge cause the stability of rhKGF. Due to heparin's narrow therapeutic margin, it is critical to understand these DDIs; thus, in this study, the interactions between rhKGF and heparin types were evaluated at the atomic levels by employing a well-established set of computational methods such as molecular docking and molecular dynamic (MD) simulations. Also, the principal component analysis (PCA), binding free energies, and the influence of synergistic heparin types on structure and biostability of rhKGF were studied *in silico*.

2 | MATERIALS AND METHODS

2.1 | Protein selection and preparation

According to a previous study, the high-quality homology model of rhKGF was prepared using the crystallographic structure of the KGF protein of *Rattus norvegicus* (PDB ID: 1QQK), as that described previously.[23] The modeled rhKGF protein structure was then prepared; by removing water molecules, adjusting atoms to AutoDock atom types, assigning bond orders, and adding hydrogen atoms and Gasteiger-Marsili charges to the protein structure using AutoDock Tools 4.2.[24] Finally, the prepared protein structure was saved in PDBQT format for molecular docking.

2.2 | Binding pocket selection and preparation

The three-dimensional (3-D) structure of the KGF-heparin complex has not yet been experimentally determined, only the crystallographic structure of the FGF1-FGFR2-heparin complex (PDB ID: 1E0O) has been solved; therefore, we were applied this crystallographic structure as template for finding the binding pocket. This crystal structure file was studied in detail by means of PDBsum web tools and Pymol as well as LigPlot softwares[25–27] and then the most significant residues

involved in the interaction of FGF1 with heparin were investigated. Subsequently, in order to find the heparin-binding site of rhKGF, a sequence and structure alignment between FGF1 and rhKGF were carried out. According to alignment and superimposition studies, the residues of rhKGF in the C-terminal region were selected as reference residues for molecular docking. Likewise, AutoDock tools were applied to predict a grid box of size $X = 20$ Å, $Y = 20$ Å, and $Z = 20$ Å grid points in 1.000 Å grid spacing around the selected binding pocket to provide a search space for the selected compounds during the molecular docking process.

2.3 | Ligand selection and preparation

There are three forms of heparin: unfractionated heparin (UH), low-molecular weight heparin (LMWH), and ultra-low molecular weight heparin (ULMWH) with average molecular weights of 15, 6, and 2 kDa, respectively.[28,29] In this study, an UH which named heparin and some of its LMWH derivatives such as enoxaparin, bemiparin, fondaparinux, and idraparinux[30] were selected as ligands. Subsequently, all these ligands were energetically minimized using HyperChem (version 7.0) with molecular mechanics using MM+ force field[31] followed by semi-empirical quantum mechanics AM1 method, available in HyperChem,[32] the Optimized ligands were then converted to SDF format using Open Babel software[33] for docking with the receptor.

2.4 | Molecular docking studies

To evaluate the molecular interaction between rhKGF and ligands, flexible docking was carried out using the Smina AutoDock program[34] under Linux OS. Subsequently, the docking results were visualized and analyzed using Pymol and LigPlot softwares.[26,27]

2.5 | Molecular dynamics simulations for protein–ligand complexes

Molecular dynamics simulations (MDs) have been widely used to assess the atom's behavior and structural stability of protein–protein and protein–ligand complexes, which prepared by molecular docking.[35,36] In this step, MDs of the rhKGF-ligand complexes were performed using GROMACS software (version 2020). The topology files of the ligands were prepared using the PRODRG server.[37] In parallel, the topology file of the receptor was generated with pdb2gmx by means of the united-atom GROMOS 96 43A1 force field. The MDs methodology carried out the same as the previous studies[23,38]; in summary, equilibration steps were set at 300 K for 100 ps using NVT (constant number of particles, volume, and temperature) following 100 ps using NPT (constant number of particles, pressure, and temperature). Finally, the equilibrated system was subjected to MDs for 100 ns.

2.6 | Principal component analysis

Correlated motions in biomolecules play an essential role in molecular function. One of the most popular methods for detecting important motions in proteins is principal component analysis (PCA) method.[39] Interestingly, GROMACS software provides PCA tools to analyze protein trajectories. In this study to calculate PCA, first, a covariance matrix was made by using gmx-covar from the equilibrated simulated time of the trajectory. Subsequently, a set of eigenvectors and eigenvalues were identified from the generated matrix by gmx-anaeig of GROMACS.

2.7 | Binding energy analysis using MM-PBSA approach

Binding free energy computations are highly dependent on the conformation of the ligand interacting with the receptor residues. The method of molecular mechanics-PoissonBoltzmann surface area (MM-PBSA) is widely applied to estimate the binding free energy of biomolecular complexes in the ending phases of the drug discovery process.[38,40,41] In the present study, this method was applied to calculate the interaction energy between the ligand and the residues in the protein binding pocket. The binding free energy was calculated by taking different energetic parameters including the Van der Waals (ΔE_{vdw}), the electrostatic (ΔE_{ele}), and the solvation (ΔG_{sol}) contributions. For each complex, the last 10 000 ps (10 ns) of the MD trajectories were selected to calculate the binding free energies. In order to determine binding free energies, a set of equations was computed as follow:

1. $\Delta G_{bind} = G_{complex} - (G_{protein} + G_{ligand})$
2. $\Delta G_{bind} = \Delta E_{MM} - T\Delta S + \Delta G_{sol}$
3. $\Delta E_{MM} = \Delta E_{ele} + \Delta E_{vdw}$
4. $G_{sol} = G_{pol} + G_{nonpol}$
5. $G_{nonpol} = \gamma \Delta SASA + b$

$G_{complex}$, $G_{protein}$, and G_{ligand} represent the total free energy of the protein–ligand complex, and the total free energy of the protein and ligand in the solvent, respectively. Molecular Mechanics (MM) force-field parameters were applied to calculate complete binding energy counting the solvation of the ligand and unbound protein. So, ΔE_{MM} is the average molecular mechanic's potential energy in vacuum, $T\Delta S$ is the solute entropic contribution at temperature T (Kelvin), and G_{sol} refers to the free energy of solvation. The solvation energy (G_{sol}) was computed by summing the electrostatic (G_{pol}) and nonelectrostatic (G_{nonpol}) solvation energies. The polar solvation energies and the non-polar solvation energies were calculated by solving the linear Poisson–Boltzmann equation and by calculating solvent accessible surface area (SASA), respectively. In the last equation γ and b are a coefficient of surface tension and a fitting parameter, respectively.[23,42,43]
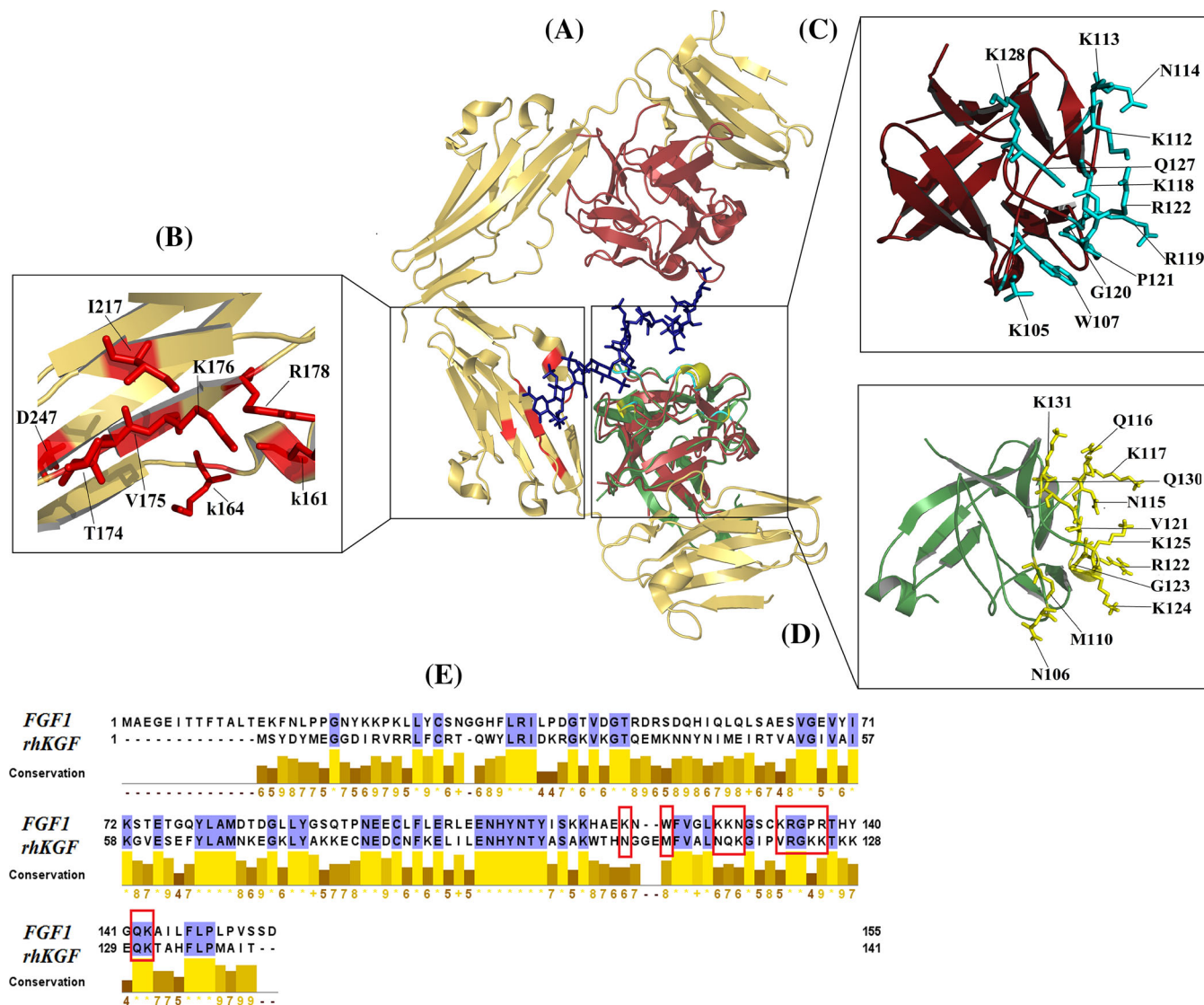
FIGURE 1 Evaluation of the heparin binding pocket upon FGF1-FGFR2-heparin complex and rhKGF. (A) Structural alignment of the FGFR2 (gold)-FGF1 (firebrick)-heparin (blue) complex (PDB ID: 1EO0) and rhKGF (green). The binding residues of FGF1 and FGFR2 are colored in cyan and red, respectively, as well as the predicted binding residues of rhKGF are colored yellow. (B) Close-up view of the interacting residues of FGFR2 (C) and FGF1 (D) as well as rhKGF which these residues are labeled and shown in stick representation. (E) Sequence alignment of FGF1 and rhKGF. Red boxes indicate heparin-interacting residues in both FGF1and rhKGF.

3 | RESULTS

3.1 | Identification of the heparin binding pocket of rhKGF

In this step to determine the heparin-binding pocket of rhKGF for molecular docking, the only crystallography file available in the PDB database with PDB ID: 1E0O (FGF1-FGFR2-heparin complex) was studied. The more detailed study of the crystallographic structure shows that a heparin decasaccharide molecule simultaneously binds to two FGF1 molecules and only one chain of the FGFR2 receptor. The heparin binding site of FGF1 including; Lys112, Lys113, Asn114, Lys118, Arg119, Pro121, Arg122, Gln127, and Lys128 residues and the heparin binding site of FGFR2 including; Lys161, Lys164,

Thr174, Val175, Lysl76, Arg178, Ile217, and Asp247 residues that were involved in FGF1-heparin and FGFR2-heparin interactions, respectively. For identifying the heparin-binding site of rhKGF, sequence and structure alignment between FGF1 and rhKGF were carried out (Figure 1). According to alignment and superimposition studies, the Asn106, Met110, Asn115, Glu116, Lys117, Val121, Arg122, Gly123, Lys124, Lys125, Glu130, and Lys131 residues in the C-terminal region of rhKGF were chosen as binding pocket. Also, the evaluation of the electrostatic surface of FGF1 represented that the heparin binding site of FGF1 is positively charged (data not shown). Accordingly, the selected residues of rhKGF as binding pocket were also positively charged so that they might make a strong electrostatic connection with the negatively charged heparin and LMWH derivatives.

TABLE 1 Evaluation of the binding affinity (kcal/mol) and interacting residues in the rhKGF-ligand complexes.

Names compound	Binding affinity (kcal/mol)	HB-AAs[a]	NH-AAs[b]
Heparin	−6.0	Asn115, Gln116, Arg122, Lys124, Lys125	Leu114, Ile119, Pro120, Gly123, Thr126, Gln130, Thr1321
Bemiparin	−5.7	Asn115 Lys127, Gln130	Ile119, Pro120, Val121, Arg122, Thr126, Thr132
Fondaparinux	−5.7	Asn115, Lys125, Lys127	Leu114, Gln116, Gln130, Thr132
Enoxaparin	−5.4	Asn115, Gln116, Lys125, Gln130	Leu114, Val121, Arg122, Gly123, Thr126, Glu129, Thr132
Idraparinux	−6.9	Asn115, Lys124, Lys125, Lys127, Gln130	Ile119, Val121, Arg122, Gly123, Thr126

[a]Hydrogen bonds forming amino acids.
[b]Nonbonded contacts forming amino acids.
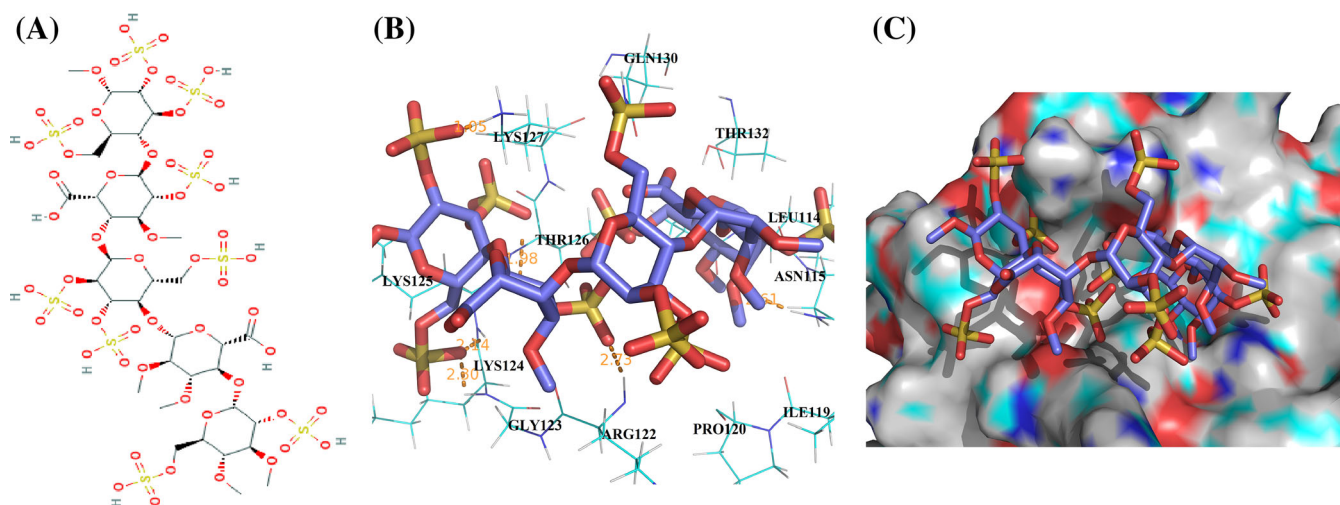
FIGURE 2 Two-dimensional (2-D) structure of heparin and three-dimensional illustration of its interaction with the heparin binding pocket of rhKGF. (A) Presents the 2-D structure of heparin. (B) Shows residues involved in hydrogen and hydrophobic interactions in protein–ligand complex, hydrogen bonds represented as yellow dotted lines. (C) Represents eparin in the binding pocket of rhKGF. Heparin is shown as blue sticks; all pictures were prepared with Pymol.

3.2 | Assessment of binding modes of heparin and LMWH derivatives interactions with rhKGF

In this step, the rhKGF complex with heparin and LMWH derivatives was evaluated based on the docking energy, number of hydrogen bonds and interacting residues. The rhKGF-heparin complex showed a binding affinity of −6.0 kcal/mol, while the rhKGF-idraparinux complex displayed the highest binding affinity (−6.9 kcal/mol). The complexes of bemiparinand and fondaparinux with rhKGF represented the same binding affinity (−5.7 kcal/mol); likewise, rhKGF-enoxaparin complex had the lowest binding affinity (−5.4 kcal/mol). More details about the binding affinity and interacting residues in the rhKGF-ligand complexes are given in Table 1.

The analysis of heparin binding to rhKGF demonstrated that seven hydrogen bonds formed between the amine group of heparin and Asn115 (angle O---H—N = 160.13°, distance = 2.61 Å), Gln116 (angle O---H—N = 152.54°, distance = 2.22 Å), Arg122 (angle O---H—N = 140.92°, distance = 2.73 Å), Lys124 (angle O---H—N = 114.53°,

distance = 2.30 Å), Lys125 (angle O---H—N = 134.56°, distance = 2.14 Å), Lys125 (angle O---H—N = 108.35°, distance = 1.98 Å), Lys127 (angle O---H—N = 163.41°, distance = 1.05 Å) residues in the binding pocket of rhKGF. In addition, heparin was embedded in a hydrophobic pocket formed by, Leu114, Ile119, Pro120, Gly123, Thr126, Gln130, and Thr132 amino acids (Figure 2).

Analysis of rhKGF-bemiparin complex showed that five hydrogen bonds formed between amine group of bemiparin and Asn115 (angle O---H—N = 154.78°, distance = 2.19 Å), Asn115 (angle O---H—N = 76.12°, distance = 2.99 Å), Lys127 (angle O---H—N = 147.19°, distance = 3.10 Å), Lys127 (angle O---H—N = 114.04°, distance = 2.18 Å), Gln130 (angle O---H—N = 97.49°, distance = 2.68 Å), residues in the binding pocket of rhKGF. In addition, bemiparin was embedded in a hydrophobic pocket formed by, Ile119, Pro120, Val121, Arg122, Thr126, and Thr132 amino acids (Figure 3).

Based on the docking results, three hydrogen bonds formed between the amine group of fondaparinux and Asn115 (angle O---H—
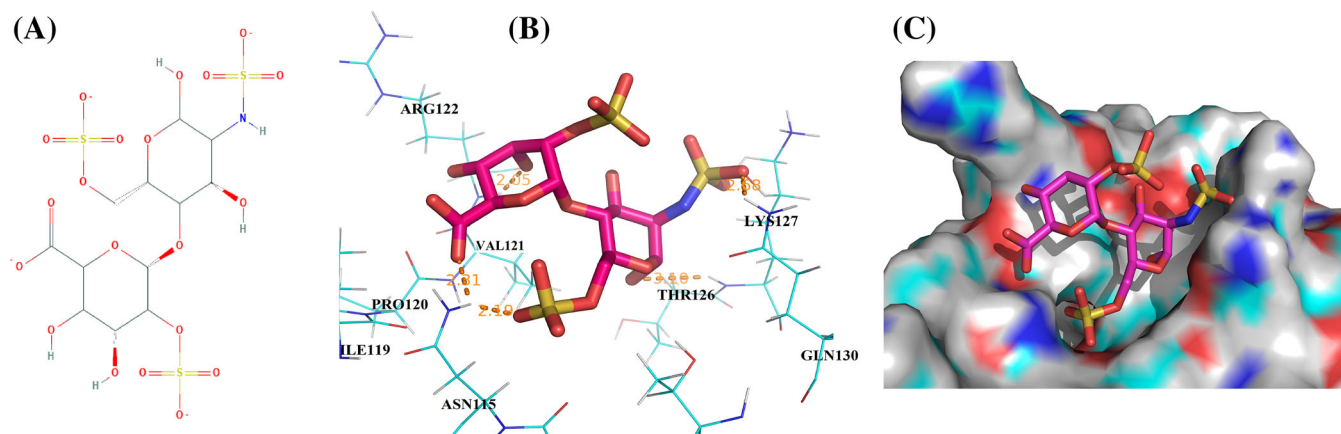
FIGURE 3 Two-dimensional (2-D) structure of bemiparin and three-dimensional illustration of its interaction with the heparin binding pocket of rhKGF. (A) Presents the 2-D structure of bemiparin. (B) Shows residues involved in hydrogen and hydrophobic interactions in protein–ligand complex, hydrogen bonds represented as yellow dotted lines. (C) Represents bemiparin in the binding pocket of rhKGF. Bemiparin is shown as magenta sticks; all pictures were prepared with Pymol.
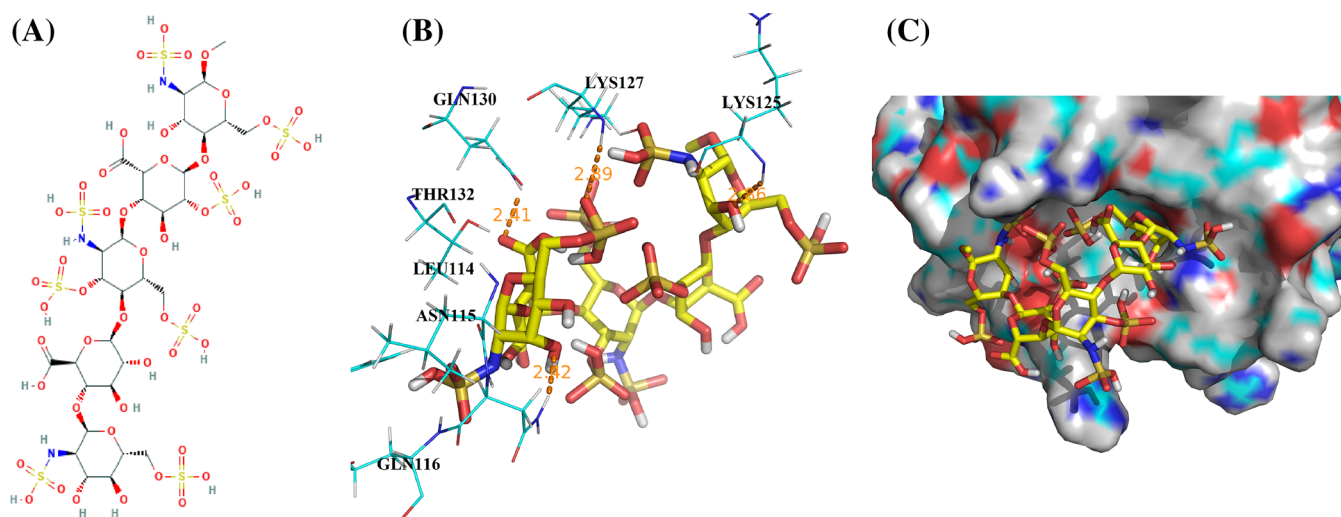

FIGURE 4 Two-dimensional (2-D) structure of fondaparinux and three-dimensional illustration of its interaction with the heparin binding pocket of rhKGF. (A) Presents the 2-D structure of fondaparinux. (B) Shows residues involved in hydrogen and hydrophobic interactions in protein–ligand complex, hydrogen bonds represented as yellow dotted lines. (C) represents fondaparinux in the binding pocket of rhKGF. Fondaparinux is shown as yellow sticks, all pictures were prepared with Pymol.

N = 143.56°, distance = 2.42 Å), Lys125 (angle O---H—N = 146.95°, distance = 2.86 Å), Lys127 (angle O---H—N = 166.74°, distance = 2.89 Å), Gln130 (angle O---H—N = 113.40°, distance = 2.41 Å) residues in the binding pocket of rhKGF. In addition, fondaparinux was embedded in a hydrophobic pocket formed by, Leu114, Gln116, Gln130, and Thr132 amino acids (Figure 4).

Detailed study of the docking results of enoxaparin revealed that eight hydrogen bonds formed between the oxygens (C=O) of enoxaparin and Asn115 (angle O---H—N = 127.31°, distance = 2.46 Å), Asn115 (angle O---H—N = 90.11°, distance = 2.95 Å), Gln116 (angle O---H—N = 152.10°, distance = 2.28 Å), Lys125 (angle O---H—N = 154.38°, distance = 2.12 Å), Lys127 (angle O---H—N = 174.38°, distance = 2.00 Å), Lys127 (angle O---H—N = 101.70°, distance = 2.54 Å), Gln130 (angle O---H—N = 113.40°,

distance = 2.57 Å), Gln130 (angle O---H—N = 136.57°, distance = 2.56 Å), residues in the binding pocket of rhKGF. In addition, enoxaparin was embedded in a hydrophobic pocket formed by, Leu114, Val121, Arg122, Gly123, Thr126, Glu129, and Thr132 amino acids (Figure 5).

Analysis of the docking results of the rhKF-idraparinux complex displayed that six hydrogen bonds formed between various oxygens (—O— and C=O) of idraparinux and Asn115 (angle O---H—N = 145.63°, distance = 2.22 Å), Asn115 (angle O---H—N = 96.57°, distance = 2.71 Å), Lys124 (angle O---H—N = 168.15°, distance = 2.34 Å), Lys125 (angle O---H—N = 130.69°, distance = 2.24 Å), Lys127 (angle O---H—N = 161.88°, distance = 1.88 Å), Gln130 (angle O---H—N = 164.86°, distance = 1.90 Å) residues in the binding pocket of rhKGF. In addition, idraparinux was

FIGURE 5 Two-dimensional (2-D) structure of enoxaparin and three-dimensional illustration of its interaction with the heparin binding pocket of rhKGF. (A) Presents the 2-D structure of enoxaparin. (B) Shows residues involved in hydrogen and hydrophobic interactions in protein–ligand complex, hydrogen bonds represented as yellow dotted lines. (C) Represents enoxaparin in the binding pocket of rhKGF. Enoxaparin is shown as orange sticks; all pictures were prepared with Pymol.
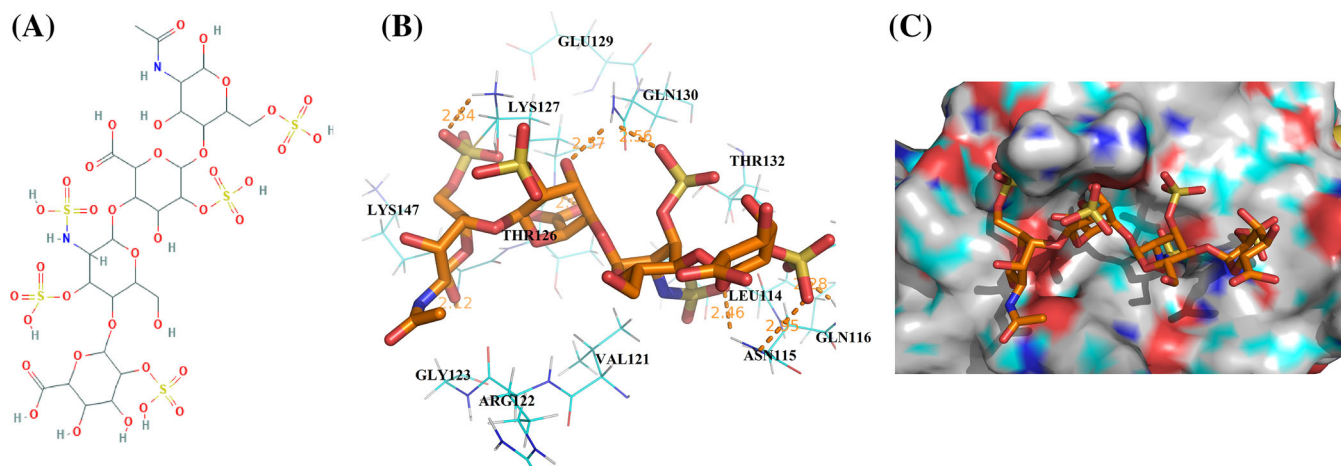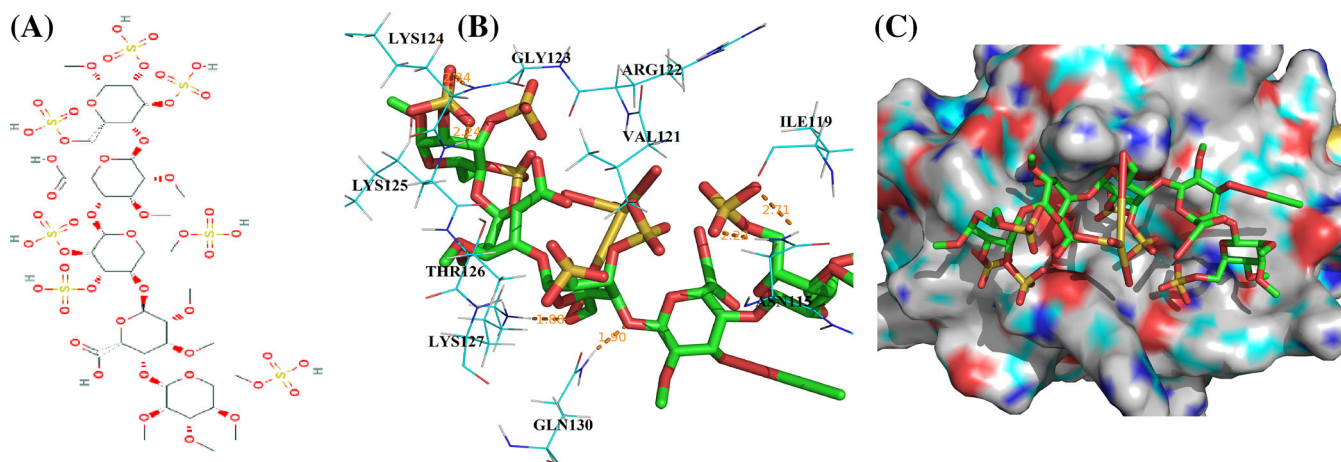

FIGURE 6 Two-dimensional (2-D) structure of idraparinux and three-dimensional illustration of its interaction with the heparin binding pocket of rhKGF. (A) Presents the 2-D structure of idraparinux. (B) Shows residues involved in hydrogen and hydrophobic interactions in protein–ligand complex, hydrogen bonds represented as yellow dotted lines. (**C**) Represents idraparinux in the binding pocket of rhKGF. Idraparinux is shown as green sticks; all pictures were prepared with Pymol.

embedded in a hydrophobic pocket formed by Ile119, Val121, Arg122, Gly123, and Thr126 amino acids (Figure 6).

3.3 | Molecular dynamic simulations

Molecular dynamics were performed to evaluate the stability of rhKGF-ligand complexes during 100 ns simulations. Root mean square deviation (RMSD) is the significant property to evaluate the conformational changes and dynamic behavior of the protein structure. The RMSD plots for rhKGF-ligand complexes during the simulation period are illustrated in Figure 7A. The result of the RMSD value showed that the most deviation belongs to the rhKGF-enoxaparin complex; however, it displayed slight fluctuation from 10 000 to 50 000 ps. The

RMSD value of the rhKGF-fondaparinux complex was approximately stable (around 0.25–0.28 nm) during 10 000–50 000 ps, but it increased around 0.3–0.33 nm and 0.35–38 nm during 51 000–81 000 ps and 84 000–100 000 ps, respectively. The RMSD value for the rhKGF-heparin complex was in the range of 0.15–0.30 nm during the simulations, while this value for the rhKGF-bemiparin complex was fluctuated from 0.15 to 0.25 nm then increased slightly and persisted at 0.30 nm from 90 000 ps till the end of the simulation. Also, the RMSD value for the rhKGF-idraparinu complex was fluctuated from 0.15 to 0.30 nm and then reached its steady state at 0.25 nm from 45 000 ps till the end of the simulation. The results demonstrated the pattern of changes in RMSD was almost similar for three complexes; rhKGF-heparin, rhKGF-bemiparin and rhKGF-idraparinux which displayed the least fluctuation of RMSD plot during MDs;
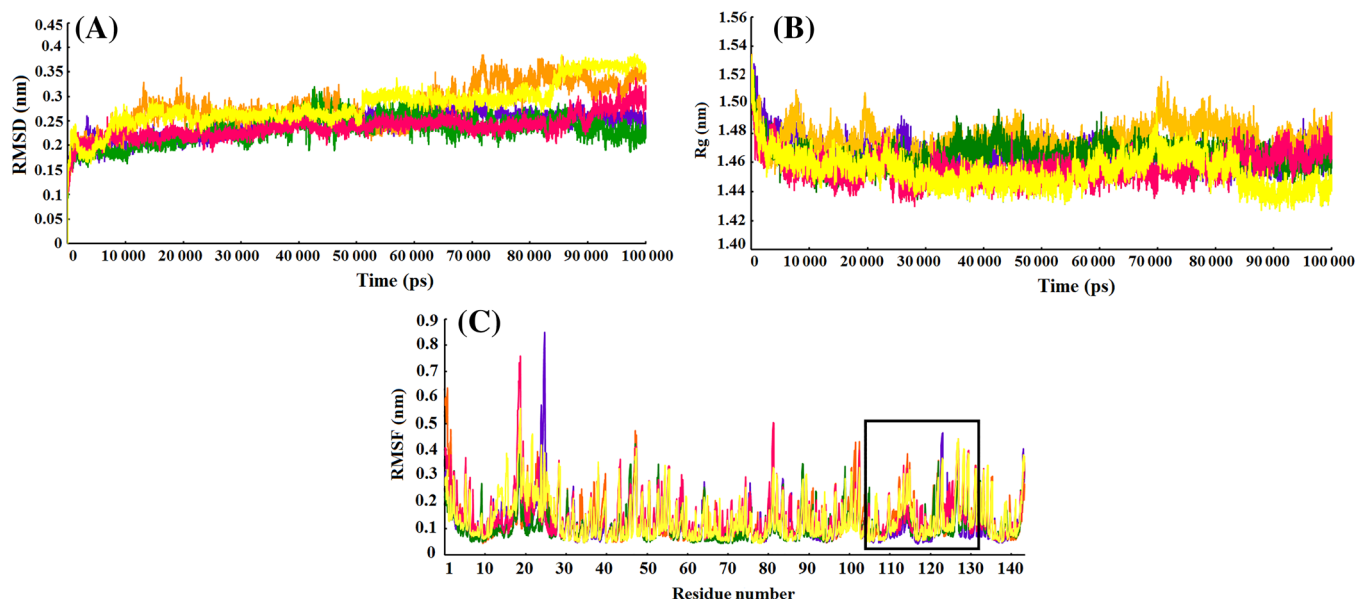
FIGURE 7 Evaluation of molecular dynamic (MD) simulations results. (A) Root mean square deviation (RMSD) plots of the rhKGF-ligand complexes during 100 ns of simulations. (B) Radius of gyration (R_g) plots of the rhKGF-ligand complexes during MD simulations. (C) Root mean square fluctuation (RMSF) plots of the rhKGF-ligand complexes. In all plots, rhKGF-heparin, rhKGF-bemiparin, rhKGF-fondaparinux, rhKGF-enoxaparin, and rhKGF-idraparinux complexes are indicated as blue, magenta, yellow, orange, and green, respectively.

although rhKGF-bemiparin had lower RMSD values, rhKGF-heparin had higher stability than other complexes at the last 10 000 ps. In order to evaluate protein structure compactness during the simulation, radius of gyration (R_g) value of the complexes was calculated. As depicted in Figure 7B, rhKGF-enoxaparin and rhKGF-fondaparinux complexes had the highest fluctuation, but the R_g value of both decreased during the last 30 000 ps. The pattern of changes in R_g is almost similar for rhKGF-heparin, rhKGF-bemiparin, and rhKGF-idraparinux complexes; however, the rhKGF-bemiparin complex displayed the least R_g value throughout the simulation periods.

To study the flexibility of individual residues, root mean square fluctuation (RMSF) value was calculated from the trajectories of each complex (Figure 7C). The RMSF value of the rhKGF-heparin complex uncovered that all residues fluctuated between 0.04 and 0.85 nm and this value in the rhKGF-bemiparin complex was in the range of 0.05–0.75 nm during simulations. Also, the RMSF value for the rhKGF-idraparinu, rhKGF-enoxaparin, and rhKGF-fondaparinux complexes was fluctuated from 0.04 to 0.42 nm, 0.04 to 0.63 nm, and 0.05 to 0.55 nm, respectively. The RMSF plot of the complexes showed that all residues played in the binding pocket of rhKGF were fluctuated between 0.05 and 0.45 nm, indicating that these residues can have high interaction with selected heparin and LMWH derivatives throughout MDs.

The results of calculation of the number of hydrogen bonds (H-bonds) between the rhKGF and ligands during MDs showed that the complexes of rhKGF with heparin and idraparinux possessed 0–7 and 0–5 H-bonds, respectively, while rhKGF-bemiparin, rhKGF-enoxaparin, and rhKGF-fondaparinux complexes had 0–6 H-bonds. In all of the complexes, 2–3 H-bonds were averagely seen which were strongly stable during MDs (Figure 8A).

However, the SASA was investigated to define the surface area of the protein interacting with its solvent molecules. Average SASA values for rhKGF-heparin, rhKGF-bemiparin, rhKGF-fondaparinux, rhKGF-enoxaparin, and rhKGF-idraparinux complexes were found to be 85, 83, 81, 84, and 86 nm^2, respectively during 100 ns MD simulations (Figure 8B). Also, standard deviation of the area over the trajectory were calculated per atom. The standard deviation' atoms values for rhKGF-heparin, rhKGF-bemiparin, rhKGF-fondaparinux, rhKGF-enoxaparin, and rhKGF-idraparinux complexes were 0.55, 0.48, 0.48, 0.5, and 0.47 nm^2, respectively during 100 ns. The results of SASA showed that there was no major change in the SASA values owing to ligands binding.

In this study, the correlated motions for ligands binding to rhKGF were anticipated by PCA. The first 20 eigenvectors were selected for the investigation. The results showed that the eigenvalue Plot is diminishing against the corresponding eigenvector for all complexes. It can be seen that the rhKGF-enoxaparin complex had the highest motions as compared to the other complexes while the complexes of heparin and idraparinux with rhKGF showed lower motions, all these computations were carried up at the last 50 ns MD trajectories. From the overall analysis, it is predicted that the ligands of heparin and idraparinux could form a more stable complex with rhKGF (Figure 9A).

In order to study the essential dynamics of the complexes and to display different and detailed conformation waves, a 2-D projection plot was evaluated. In this regard, the first two eigenvectors (PC1 and PC2) were chosen and plotted against each other. The 2-D projection plot of the conformational changes of the complexes was plotted from the last 50 ns MD trajectories (Figure 9B).

In general, proteins perform their specific functions via collective atomic motions; therefore, the 2-D projection plot clearly describes
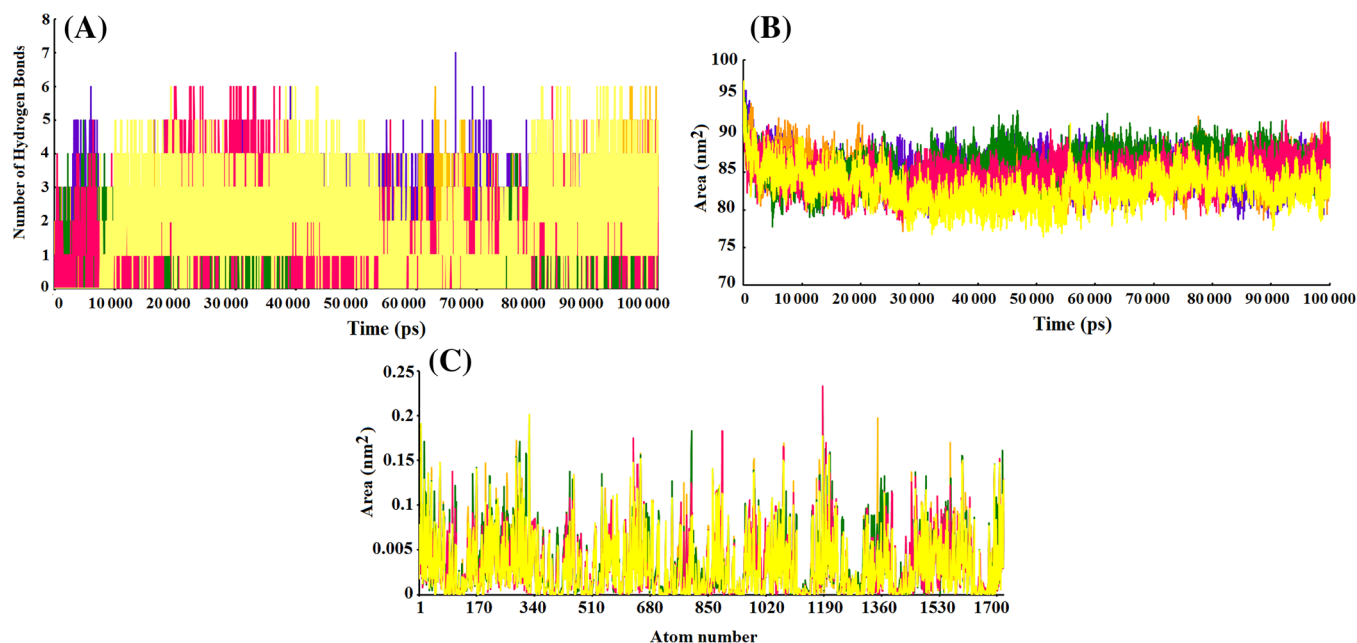
FIGURE 8 Evaluation of H-bonds and solvent accessible surface area (SASA) values for rhKGF-ligand complexes. (A) The number of H-bonds between the rhKGF and ligands as a function of time. (B) SASA of rhKGF-ligand complexes as a function of time. (C) Standard deviation of the area over the trajectory for per atom. In all plots, rhKGF-heparin, rhKGF-bemiparin, rhKGF-fondaparinux, rhKGF-enoxaparin, and rhKGF-idraparinux complexes are indicated as blue, magenta, yellow, orange, and green, respectively.

the motions in the protein in a phase space to understand the stability of the protein.[44] In this regard, the first two eigenvectors (PC1 and PC2) were chosen and plotted against each other (Figure 9B). The 2-D plot results of the complexes clearly represent that the rhKGF-heparin and rhKGF-idraparinux complexes covered an almost smaller region of the phase space, while rhKGF-enoxaparin, rhKGF-bemiparin, and rhKGF-fondaparinux complexes occupied a larger region of the phase space. Therefore, the PCA results suggest that rhKGF-heparin and rhKGF-idraparinux complexes are more stable than other complexes, in other words, rhKGF-enoxaparin, rhKGF-bemiparin, and rhKGF-fondaparinux complexes have more structure flexibility and dynamics at the last 50 MD.

To study the correlated motions in more detail, eigenvalue Plots were calculated for shorter time periods (for the at last 10 ns MD trajectories) which were then this plot compared with the eigenvalue Plots at the last 50 ns. The results showed that the rhKGF-enoxaparin and heparin and idraparinux had the highest and lower motions, respectively (Figure 9C). Also, the 2-D plot results of the complexes during at the last 50 and 10 ns MD trajectories were approximately the same (Figure 9D). From the results of this study, it can be concluded that the rhKGF-heparin and rhKGF-idraparinux complexes showed the least fluctuations during the MD simulations.

Detailed analysis of binding free energies (ΔG_{bind}) and energy components, including van der Waals (ΔE_{vdw}), electrostatic (ΔE_{ele}), polar solvation energy (ΔG_{pol}), and nonpolar interactions (ΔG_{nonpol}) were computed to assay the most important interaction term which impacts the computed binding energy by using MM-BPSA method

throughout the last 10 000 ps MD trajectories. The results of the energy components of the complexes are tabulated in Table 2.

The calculated average value of ΔG_{bind} for rhKGF-idraparinux, rhKGF-heparin, rhKGF-fondaparinux, rhKGF-enoxaparin, and rhKGF-bemiparin complexes have -265.709, -261.478, -230.448, -214.183, and -163.598 kJ/mol, respectively. The ΔG_{bind} results suggested that idraparinux and heparin have the highest affinity for rhKGF. In general, the nonpolar interaction energies and polar interaction energies were calculated by ($\Delta E_{vdw} + \Delta G_{nonpolar}$) and ($\Delta E_{ele} + \Delta G_{polar}$), respectively.[45–47] The nonpolar interaction energies ($\Delta E_{vdw} + \Delta G_{nonpolar}$) of the rhKGF-idraparinux, rhKGF-heparin, rhKGF-fondaparinux, rhKGF-enoxaparin, and rhKGF-bemiparin systems were found to be -384.778, -316.43, -375.328, -282.18, and -213.351 kJ/mol, respectively, indicating that hydrophobic interactions contribute to the binding process. The polar interaction energies ($\Delta E_{ele} + \Delta G_{polar}$) of the rhKGF-idraparinux (119.069 kJ/mol), rhKGF-heparin (54.952 kJ/mol), rhKGF-fondaparinux (144.88 kJ/mol), rhKGF-enoxaparin (67.997 kJ/mol), and rhKGF-bemiparin (49.753 kJ/mol) systems unfavorable for protein–protein complex formation.

4 | DISCUSSION

Since the KGF could operate as a hemostatic agent to maintain the accretion and stability of epithelial cells and also have a main role in tissue repair and preservation of the mucosal barrier, it is distinct from other FGFs and provides a significant field for therapeutic
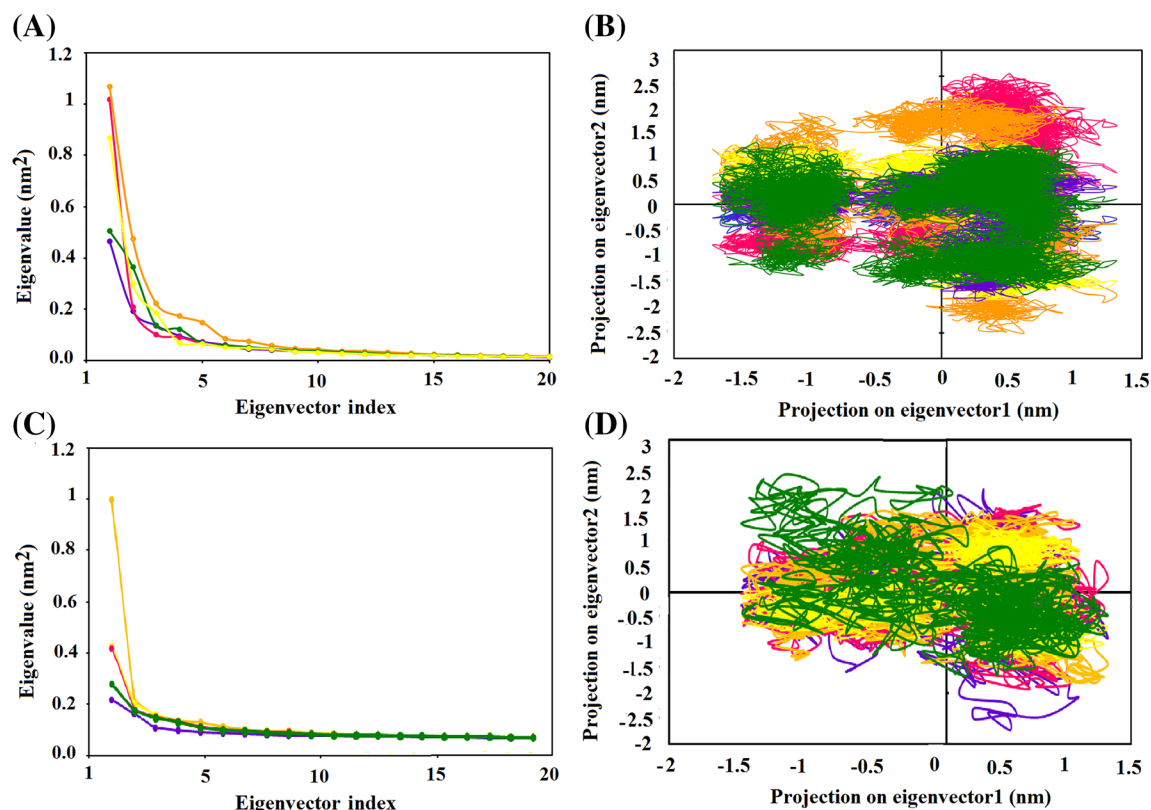
FIGURE 9 Evaluation of principal component analysis (PCA) results. (A) Eigenvalue plot versus the eigenvector index, considering only the first 20 eigenvectors and (B) Projection plot of the motion of the rhKGF in phase space along the first two principal component vectors, PC1 and PC2 at the last 50 ns. (C) Eigenvalue plot versus the eigenvector index, considering only the first 20 eigenvectors and (D) Projection plot of the motion of the rhKGF in phase space along the first two principal component vectors, PC1 and PC2 at the last 10 ns. In all plots, rhKGF-heparin, rhKGF-bemiparin, rhKGF-fondaparinux, rhKGF-enoxaparin, and rhKGF-idraparinux complexes are indicated as blue, magenta, yellow, orange, and green, respectively.

TABLE 2 Analysis of the binding free energies (kJ/mol) and energy components (kJ/mol) in the rhKGF-ligand complexes.

Names compound	ΔE_{vdw}[a]	ΔE_{ele}[b]	ΔG_{pol}[c]	$\Delta G_{nonpolar}$[d]	ΔG_{bind}[e]	$\Delta E_{vdw} + \Delta G_{nonpolar}$	$\Delta E_{ele} + \Delta G_{polar}$
Heparin	−293.901	−62.365	117.317	−22.529	−261.478	−316.43	54.952
Bemiparin	−197.964	−20.841	70.594	−15.387	−163.598	−213.351	49.753
Fondaparinux	−348.211	−54.986	199.866	−27.117	−230.448	−375.328	144.88
Enoxaparin	−261.581	−83.960	151.957	−20.599	−214.183	−282.18	67.997
Idraparinux	−354.937	−72.173	191.242	−29.841	−265.709	−384.778	119.069

Note: $\Delta G_{bind} = \Delta E_{vdw} + \Delta E_{ele} + \Delta G_{pol} + \Delta G_{nonpol}$.
[a]E_{vdw}, van der Waals contribution.
[b]ΔE_{ele}, electrostatic contribution.
[c]ΔG_{pol}, polar solvation energy.
[d]ΔG_{nonpol}, nonpolar solvation energy.
[e]ΔG_{bind}, binding energy.

applications. Based on these unique properties, recombinant human KGF protein (rhKGF) has been used for several therapeutic targets. It is well documented that rhKGF has been successful in the decrease of chemotherapy and radiotherapy toxicities in cancer patients. Several factors such as instability, aggregation and short half-life, limited the clinical applications of rhKGF. Yang et al. evaluated DDIs using an *in vitro* model, they assessed rhKGF–heparin interactions in terms of

pharmacokinetics and pharmacodynamics characteristics. They reported that the coadministration of rhKGF and UH may result in a 4 to 5-fold increase in some rhKGF's pharmacokinetic characteristics whereas the pharmacodynamic characteristics are unaffected.[22] However, in the previous studies, there has not been a focus on evaluating the synergistic effect of heparin types in improving stability and bioactivity of rhKGF on atomic level. Since heparin's narrow therapeutic

margin, scrutiny of the effect of heparin types on rhKGF is critical; therefore, in this study, for the first-time evaluated the atomic interactions of heparin types with rhKGF. Because of the experimental methods for investigating these interactions are expensive and time-consuming, we applied computational approaches to investigate the effect of heparin and LMWH derivatives on rhKGF and also, deeply assess their features, differences, and interaction. Molecular docking was performed by using AutoDock Vina tools; between flexible residues of the selected binding pocket of rhKGF (Asn106, Met110, Asn115, Glu116, Lys117, Val121, Arg122, Gly123, Lys124, Lys125, Glu130, and Lys131 residues) and selected ligands (heparin and LMWH derivatives). The results of molecular docking showed a favorable binding affinity for the rhKGF-heparin complex. As for the LMWH derivatives, it was found that the binding affinity of heparin (−6.0) and idraparinux (−6.9) was better compared to other selected LMWH derivatives.

Interaction analysis of the ligands with rhKGF, revealed that heparin and idraparinux had interacted with maximum numbers of target residues; heparin interacted whit Asn115, Gln116, Arg122, Lys124, Lys125, Leu114, Ile119, Pro120, Gly123, Thr126, Gln130, and Thr1321 residues and idraparinux interacted with Asn115, Lys124, Lys125, Lys127, Gln130, Ile119, Val121, Arg122, Gly123, and Thr126 residues as compared to other ligands (Table 1).

The MD simulations analyses of the rhKGF and ligand complexes discovered that all ligands formed stable complexes with rhKGF during the simulation periods. However, the rhKGF-heparin, rhKGF-bemiparin, and rhKGF-idraparinux complexes maintained less fluctuations than the rhKGF-fondaparinux, rhKGF-enoxaparin complexes (Figures 7 and 8).

It has been documented in the drug bank that coadministration of rhKGF with bemiparin lead to an increase in the serum concentration of rhKGF. Accordingly, the RMSD and R_g results presented that bemiparin formed a stable complex with rhKGF during the 100 ns of simulations. Interestingly, the rhKGF-heparin and rhKGF-idraparinux complexes disclosed less fluctuations compared to rhKGF-bemiparin complex throughout MD simulations. Thus, it can be suggested that heparin and idraparinux might dramatically increase the serum concentration of rhKGF.

It is well documented that the RMSD is a feature that calculates the distance between protein atoms. The average distance between atoms in a protein permits us to evaluate the comparative conformation and stability of the protein.[48] The results showed that the systems include rhKGF-heparin, rhKGF-bemiparin, and rhKGF-idraparinux complexes presented the least fluctuation in the RMSD plot, suggesting that these systems were more stable than the rhKGF-fondaparinux, rhKGF-enoxaparin complexes during the 100 ns MDs (Figure 7A). Also, R_g is an important parameter for evaluating protein folding. The R_g plot also displayed that rhKGF-heparin, rhKGF-bemiparin, and rhKGF-idraparinux complex had the least fluctuation (Figure 7B). The RMSF parameter assess the fluctuation of protein atoms through the time duration from a reference situations.[49] In this study, the binding of heparin and LMWH derivatives showed the stabilization of the 106–131 amino acid residues (binding pocket) during the simulation time (Figure 7B).

To obtain further information about the system and structural stability, hydrogen bonds and the SASA value were analyzed in study (Figure 8). Hydrogen bonds play an important role instabilizing ligand-protein complexes so more stable complexes have more hydrogen bonds.[49] The analysis of H-bonds of heparin and LMWH derivatives during the simulation period indicated the potential stability of the protein complex; of course, idraparinux had more H-bonds with rhKGF (Figure 8A). The average and standard deviation of the results from SASA showed that the pattern of changes at SASA was almost similar for all complexes (Figure 8A,B). Also, from the PCA studies, it was observed that the interaction of heparin and idraparinux ligands with rhKGF was more stable and stronger compared to other LMWH derivatives (Figure 9). Interestingly, the MM-PBSA results of the complexes disclosed that heparin and idraparinux had stronger binding affinity with rhKGF than other LMWH derivatives. Enoxaparin and fondaparinux are a possible alternative because they show a more stable interaction with rhKGF so that they can have a better binding free energy than bemiparin. A more detailed study of the energies involved in the binding free energy revealed that Van der Waals interactions and nonpolar solvation energies provide the plentiful driving force for the binding of a ligand to the complexes (Table 2).

Considering all parameters, idraparinux represented better features compared with heparin and the other LMWH derivatives. Similarly, the rhKGF-idraparinux revealed the highest binding affinity (−6.9 kcal/mol) and the best conformation with rhKGF. Additionally, binding free energy analysis showed that idraparinux had the highest free energy of binding (−265.709 kJ/mol) Also, MDs results indicate that idraparinux have negligible conformational changes upon binding to rhKGF and interacts efficiently with the protein. Moreover, it was interesting that the assessment of physicochemical properties of heparin and LMWH disclosed that idraparinux had the highest molecular weight, highest number of H-bond acceptor, polar surface area, and rotatable bonds compared to other derivatives (Table 3). According to the results obtained in this study, it can be suggested that, unlike UH, idraparinux may have a significant effect on the pharmacokinetics (such as, AUC, CL, Vss, and half-life) and physicochemical properties (especially, bioactivity, and biostability) of rhKGF. It can even be recommended that idraparinux may have a significant synergistic effect on rhKGF in cancer patients; likewise, clinical trials need to be performed to confirm the curative effect of this LMWH.

5 | CONCLUSION

Although rhKGF plays an important role in the OM treatment after chemotherapy and radiotherapy in many cancer patients, the clinical applications of rhKGF are reduced due to its instability and production challenges. Since heparin is a crucial factor in KGF signaling pathway, not only the interaction of heparin with rhKGF needs to be investigated, but also the effect of heparin on the stability of

TABLE 3 Details of heparin and LMWH derivatives of physicochemical properties obtained from PubChem database.

| Name compound | Physicochemical properties | | | | | | | |
	PubID	MF	MW	CLP	HBA	HBD	PSA	RB
Heparin	444410	C36H60O55S9	1661.41	−11.5	55	11	861	35
Bemiparin	25244225	C12H17NO20S3-4	591.45	−5.6	21	5	376	6
Fondaparinux	5282448	C31H53N3O49S8	1508.26	−14.7	52	19	873	30
Enoxaparin	772	C26H42N2O37S5	1134.9	−10.8	38	15	652	21
Idraparinux	3083445	C38H64O49S7	1529.34	−9.6	49	9	735	35

Abbreviations: CLP, cLogP (lipophilicity); HBAs, H-bond acceptors; HBDs, H-bond donors; MF, molecular formula; MW, molecular weight (g/mol); PSA, polar surface area (A^2); PubID, PubChemCID; RBs, rotatable bonds.

rhKGF. The results of docking pose analysis and molecular interactions between rhKGF and heparin derivatives demonstrated that heparin and idraparinux had better binding affinity and conformation than bemiparin, fondaparinux, and enoxaparin. Moreover, the obtained results of MDs showed that all ligands formed stable complexes with rhKGF during the simulation periods. Of course, the rhKGF-heparin and rhKGF-idraparinux complexes had more stable than those of the other LMWH derivatives. The results of this study can be utilized to survey DDIs *in vitro* and *in vivo*, and can also provide data for next studies.

AUTHOR CONTRIBUTIONS

Hourieh Kalhor: Conceptualization; investigation; writing – original draft; methodology; data curation; software; formal analysis; validation. **Hoda Abolhasani:** Software; formal analysis; writing – original draft; methodology. **Reyhaneh Kalhor:** Writing – original draft; methodology; investigation. **Tahereh Komeili Movahhed:** Investigation; writing – original draft. **Hamzeh Rahimi:** Project administration; formal analysis; data curation; conceptualization; validation; writing – original draft; supervision; software.

ACKNOWLEDGMENTS

CONFLICT OF INTEREST

The authors declare no conflicts of interest.

PEER REVIEW

The peer review history for this article is available at https://publons.com/publon/10.1002/prot.26448.

DATA AVAILABILITY STATEMENT

Research data are not shared.

ORCID

Hamzeh Rahimi https://orcid.org/0000-0001-9425-2353

REFERENCES

1. Powell AK, Yates EA, Fernig DG, Turnbull JE. Interactions of heparin/heparan sulfate with proteins: appraisal of structural factors and experimental approaches. *Glycobiology*. 2004;14(4):17R-30R.
2. Sumanasekera WK, Nethery W, Tran L, Pillai G. Low molecular weight heparin as a therapeutic tool for cancer; special emphasis on breast cancer. *Biom J*. 2018;1:8.
3. Weiss RJ, Esko JD, Tor Y. Targeting heparin and heparan sulfate protein interactions. *Org Biomol Chem*. 2017;15(27):5656-5668.
4. Bernfield M, Götte M, Park PW, et al. Functions of cell surface heparan sulfate proteoglycans. *Annu Rev Biochem*. 1999;68(1): 729-777.
5. Perrimon N, Bernfield M. Specificities of heparan sulphate proteoglycans in developmental processes. *Nature*. 2000;404(6779):725-728.
6. Selleck SB. Proteoglycans and pattern formation: sugar biochemistry meets developmental genetics. *Trends Genet*. 2000;16(5):206-212.
7. Sarrazin S, Lamanna WC, Esko JD. Heparan sulfate proteoglycans. Cold Spring Harb Perspect Biol. 2011;3(7):a004952.
8. McDonnell AM, Lenz KL. Palifermin: role in the prevention of chemotherapy-and radiation-induced mucositis. *Ann Pharmacother*. 2007;41(1):86-94.
9. Nagarajan A, Malvi P, Wajapeyee N. Heparan sulfate and heparan sulfate proteoglycans in cancer initiation and progression. *Front Endocrinol (Lausanne)*. 2018;9:483.
10. Meneghetti MC, Hughes AJ, Rudd TR, et al. Heparan sulfate and heparin interactions with proteins. *J R Soc Interface*. 2015;12(110): 20150589.
11. PROFILE AR. AMJ 9701, KGF–Amgen, recombinant human keratinocyte growth factor, rHu-KGF. 2004.
12. Sadeghi S, Kalhor H, Panahi M, et al. Keratinocyte growth factor in focus: a comprehensive review from structural and functional aspects to therapeutic applications of palifermin. *Int J Biol Macromol*. 2021; 191:1175-1190.
13. Chen B-l, Arakawa T, Morris CF, Kenney WC, Wells CM, Pitt CG. Aggregation pathway of recombinant human keratinocyte growth factor and its stabilization. *Pharm Res*. 1994;11(11):1581-1587.
14. Ron D, Bottaro DP, Finch PW, Morris D, Rubin JS, Aaronson S. Expression of biologically active recombinant keratinocyte growth factor. Structure/function analysis of amino-terminal truncation mutants. *J Biol Chem*. 1993;268(4):2984-2988.
15. Kim PJ, Sakaguchi K, Sakamoto H, et al. Colocalization of heparin and receptor binding sites on keratinocyte growth factor. *Biochemistry*. 1998;37(25):8853-8862.
16. Poorebrahim M, Sadeghi S, Ghorbani R, et al. In silico enhancement of the stability and activity of keratinocyte growth factor. *J Theor Biol*. 2017;418:111-121.
17. Huang Z, Ni C, Chu Y, et al. Chemical modification of recombinant human keratinocyte growth factor 2 with polyethylene glycol

improves biostability and reduces animal immunogenicity. *J Biotechnol*. 2009;142(3–4):242-249.

18. Huang Z, Zhu G, Sun C, et al. A novel solid-phase site-specific PEGylation enhances the in vitro and in vivo biostabilty of recombinant human keratinocyte growth factor 1. *PLoS One*. 2012;7(5):e36423.

19. Derrick T, Grillo AO, Vitharana SN, et al. Effect of polyanions on the structure and stability of repifermin™ (keratinocyte growth factor-2). *J Pharm Sci*. 2007;96(4):761-776.

20. Chen BL, Arakawa T, Hsu E, Narhi LO, Tressel TJ, Chien SL. Strategies to suppress aggregation of recombinant keratinocyte growth factor during liquid formulation development. *J Pharm Sci*. 1994;83(12):1657-1661.

21. Chen B-L, Arakawa T. Stabilization of recombinant human keratinocyte growth factor by osmolytes and salts. *J Pharm Sci*. 1996;85(4):419-422.

22. Yang BB, Gillespie B, Smith B, et al. Pharmacokinetic and pharmacodynamic interactions between palifermin and heparin. *J Clin Pharmacol*. 2015;55(10):1109-1118.

23. Kalhor H, Sadeghi S, Marashiyan M, et al. In silico mutagenesis in recombinant human keratinocyte growth factor: improvement of stability and activity in addition to decrement immunogenicity. *J Mol Graph Model*. 2020;97:107551.

24. Morris GM, Huey R, Lindstrom W, et al. AutoDock4 and AutoDockTools4: automated docking with selective receptor flexibility. *J Comput Chem*. 2009;30(16):2785-2791.

25. Laskowski RA. PDBsum new things. *Nucleic Acids Res*. 2009;37(1):D355-D359.

26. DeLano WL. PyMOL. 2002.

27. Laskowski RA, Swindells MB. *LigPlot+: Multiple Ligand–Protein Interaction Diagrams for Drug Discovery*. ACS Publications; 2011.

28. Linhardt RJ, Gunay NS. Production and chemical processing of low molecular weight heparins. Paper presented at: Seminars in Thrombosis and Hemostasis 1999.

29. Xu Y, Liu J. Chemoenzymatic synthesis of structurally homogeneous ultra-low molecular weight heparins. Google Patents, 2013.

30. Ciccone MM, Cortese F, Corbo F, et al. Bemiparin, an effective and safe low molecular weight heparin: a review. *Vascul Pharmacol*. 2014;62(1):32-37.

31. Allinger NL. Conformational analysis. 130. MM2. A hydrocarbon force field utilizing V1 and V2 torsional terms. *J Am Chem Soc*. 1977;99(25):8127-8134.

32. Dewar MJ, Thiel W. Ground states of molecules. 38. The MNDO method. Approximations and parameters. *J Am Chem Soc*. 1977;99(15):4899-4907.

33. O'Boyle NM, Banck M, James CA, Morley C, Vandermeersch T, Hutchison GR. Open babel: an open chemical toolbox. *J Chem*. 2011;3(1):1-14.

34. Koes DR, Baumgartner MP, Camacho CJ. Lessons learned in empirical scoring with smina from the CSAR 2011 benchmarking exercise. *J Chem Inf Model*. 2013;53(8):1893-1904.

35. Kalhor H, Poorebrahim M, Rahimi H, et al. Structural and dynamic characterization of human Wnt2-Fzd7 complex using computational approaches. *J Mol Model*. 2018;24(10):1-14.

36. Kalhor H, Rahimi H, Eidgahi MRA, Teimoori-Toolabi L. Novel small molecules against two binding sites of Wnt2 protein as potential drug candidates for colorectal cancer: a structure based virtual screening approach. *Iran J Pharm Res*. 2020;19(2):160.

37. Schüttelkopf AW, Van Aalten DM. PRODRG: a tool for high-throughput crystallography of protein–ligand complexes. *Acta Crystallogr D Biol Crystallogr*. 2004;60(8):1355-1363.

38. Kalhor H, Sadeghi S, Abolhasani H, Kalhor R, Rahimi H. Repurposing of the approved small molecule drugs in order to inhibit SARS-CoV-2 S protein and human ACE2 interaction through virtual screening approaches. *J Biomol Struct Dyn*. 2022;40(3):1299-1315.

39. David CC, Jacobs DJ. Principal component analysis: a method for determining the essential dynamics of proteins. *Protein Dynamics*. Springer; 2014:193-226.

40. Marashiyan M, Kalhor H, Ganji M, Rahimi H. Effects of tosyl-L-arginine methyl ester (TAME) on the APC/c subunits: an in silico investigation for inhibiting cell cycle. *J Mol Graph Model*. 2020;97:107563.

41. Kalhor H, Sadeghi S, Marashiyan M, et al. Identification of new DNA gyrase inhibitors based on bioactive compounds from streptomyces: structure-based virtual screening and molecular dynamics simulations approaches. *J Biomol Struct Dyn*. 2020;38(3):791-806.

42. Zhou H, Wang C, Deng T, Tao R, Li W. Novel urushiol derivatives as HDAC8 inhibitors: rational design, virtual screening, molecular docking and molecular dynamics studies. *J Biomol Struct Dyn*. 2018;36(8):1966-1978.

43. Cheng P, Li J, Wang J, Zhang X, Zhai H. Investigations of FAK inhibitors: a combination of 3D-QSAR, docking, and molecular dynamics simulations studies. *J Biomol Struct Dyn*. 2018;36(6):1529-1549.

44. Amir M, Mohammad T, Kumar V, et al. Structural analysis and conformational dynamics of STN1 gene mutations involved in coat plus syndrome. *Front Mol Biosci*. 2019;6:41.

45. Hu H, Chen B, Zheng D, Huang G. Revealing the selective mechanisms of inhibitors to PARP-1 and PARP-2 via multiple computational methods. *PeerJ*. 2020;8:e9241.

46. Zhang Q, Sang F, Qian J, et al. Identification of novel potential PI3Kα inhibitors for cancer therapy. *J Biomol Struct Dyn*. 2021;39(10):3721-3732.

47. Rehman K, Munawar SM, Akash MSH, et al. Hesperidin improves insulin resistance via down-regulation of inflammatory responses: biochemical analysis and in silico validation. *PloS One*. 2020;15(1):e0227637.

48. Gupta S, Singh AK, Kushwaha PP, et al. Identification of potential natural inhibitors of SARS-CoV2 main protease by molecular docking and simulation studies. *J Biomol Struct Dyn*. 2021;39(12):4334-4345.

49. Kushwaha PP, Singh AK, Bansal T, et al. Identification of natural inhibitors against SARS-CoV-2 drugable targets using molecular docking, molecular dynamics simulation, and MM-PBSA approach. *Front Cell Infect Microbiol*. 2021;11:730288.